Probing Heme Propionate Involvement in Transmembrane Proton Transfer Coupled to Electron Transfer in Dihemic Quinol:Fumarate Reductase by ^{13}C-Labeling and FTIR Difference Spectroscopy†

Mauro Mileni,‡,§ Alexander H. Haas,‡,§ Werner Mäntele,|| Jörg Simon,⊥ and C. Roy D. Lancaster*,§

Department of Molecular Membrane Biology, Max Planck Institute of Biophysics, Max-von-Laue-Strasse 3, 60438 Frankfurt am Main, Germany, Institute of Biophysics, J. W. Goethe University, Max-von-Laue-Strasse 1, 60438 Frankfurt am Main, Germany, and Institute of Microbiology, J. W. Goethe University, Marie-Curie-Strasse 9, 60439 Frankfurt am Main, Germany

Received June 1, 2005; Revised Manuscript Received October 19, 2005

ABSTRACT: Quinol:fumarate reductase (QFR) is the terminal enzyme of anaerobic fumarate respiration. This membrane protein complex couples the oxidation of menaquinol to menaquinone to the reduction of fumarate to succinate. Although the diheme-containing QFR from *Wolinella succinogenes* is known to catalyze an electroneutral process, its three-dimensional structure at 2.2 Å resolution and the structural and functional characterization of variant enzymes revealed locations of the active sites that indicated electrogenic catalysis. A solution to this apparent controversy was proposed with the so-called "E-pathway hypothesis". According to this, transmembrane electron transfer via the heme groups is strictly coupled to a parallel, compensatory transfer of protons via a transiently established pathway, which is inactive in the oxidized state of the enzyme. Proposed constituents of the E-pathway are the side chain of Glu C180 and the ring C propionate of the distal heme. Previous experimental evidence strongly supports such a role of the former constituent. Here, we investigate a possible heme−propionate involvement in redox-coupled proton transfer by a combination of specific ^{13}C-heme propionate labeling and Fourier transform infrared (FTIR) difference spectroscopy. The labeling was achieved by creating a *W. succinogenes* mutant that was auxotrophic for the heme−precursor 5-aminolevulinate and by providing [1-^{13}C]-5-aminolevulinate to the medium. FTIR difference spectroscopy revealed a variation on characteristic heme propionate vibrations in the mid-infrared range upon redox changes of the distal heme. These results support a functional role of the distal heme ring C propionate in the context of the proposed E-pathway hypothesis of coupled transmembrane electron and proton transfer.

Quinol:fumarate reductase (QFR)[1] is the terminal enzyme of fumarate respiration (*1*, *2*), a form of anaerobic respiration that uses fumarate instead of dioxygen as the terminal electron acceptor. QFR couples the two-electron reduction of fumarate to succinate (reaction a) to the two-electron oxidation of quinol to quinone (reaction b)

$$\text{fumarate} + 2H^+ + 2e^- \rightarrow \text{succinate} \quad \text{(a)}$$

$$\text{quinol} \rightarrow \text{quinone} + 2H^+ + 2e^- \quad \text{(b)}$$

This reaction is part of an electron-transfer chain that allows the bacterium to grow with various electron-donor substrates such as formate or hydrogen (Figure 1a). In analogy to aerobic respiration (*3*), the energy released in fumarate respiration is transiently stored in the form of an electrochemical proton potential across the membrane. QFR from *Wolinella succinogenes* comprises two hydrophilic subunits (A and B) and one hydrophobic, membrane-integrated subunit C. The larger hydrophilic subunit A incorporates a covalently bound flavin adenine dinucleotide (FAD); the smaller hydrophilic subunit B contains three iron−sulfur clusters ([2Fe−2S], [4Fe−4S], and [3Fe−4S]); and the hydrophobic subunit C harbors two heme *b* groups (Figure 1b). On the basis of their relative distance to the hydrophilic subunits, these heme groups are referred to as the "proximal" heme b_P and the "distal" heme b_D, respectively. Although electrophysiological experiments performed with inverted vesicles and proteoliposomes containing QFR demonstrated that the reaction catalyzed by the diheme-containing QFR

† This work was supported by the Deutsche Forschungsgemeinschaft (SFB 472 "Molecular Bioenergetics") and the Max Planck Society. M.M. is supported by the International Max Planck Research School on the Structure and Function of Biological Membranes.

* To whom correspondence should be addressed: P.O. Box 55 03 53, 60402 Frankfurt am Main, Germany. Telephone: +49-69-6303-1013. Fax: +49-69-6303-1002. E-mail: roy.lancaster@mpibp-frankfurt.mpg.de.

‡ M.M. and A.H.H. contributed equally to this work.

§ Max Planck Institute of Biophysics.

|| Institute of Biophysics, J. W. Goethe University.

⊥ Institute of Microbiology, J. W. Goethe University.

[1] Abbreviations: ALA, 5-aminolevulinate, b_D, distal (heme) *b*; b_P, proximal (heme) *b*; DEAE, diethylaminoethyl; $DMNH_2$, 2,3-dimethyl-1,4-naphthoquinol FAD, flavin adenine dinucleotide; FTIR, Fourier transform infrared; IEF, isoelectric focusing; MB, methylene blue; PAGE, polyacrylamide gel electrophoresis; QFR, quinol:fumarate reductase; SDS, sodium dodecyl sulfate; SHE, standard hydrogen electrode.

10.1021/bi051034s CCC: $30.25
Published on Web 11/22/2005

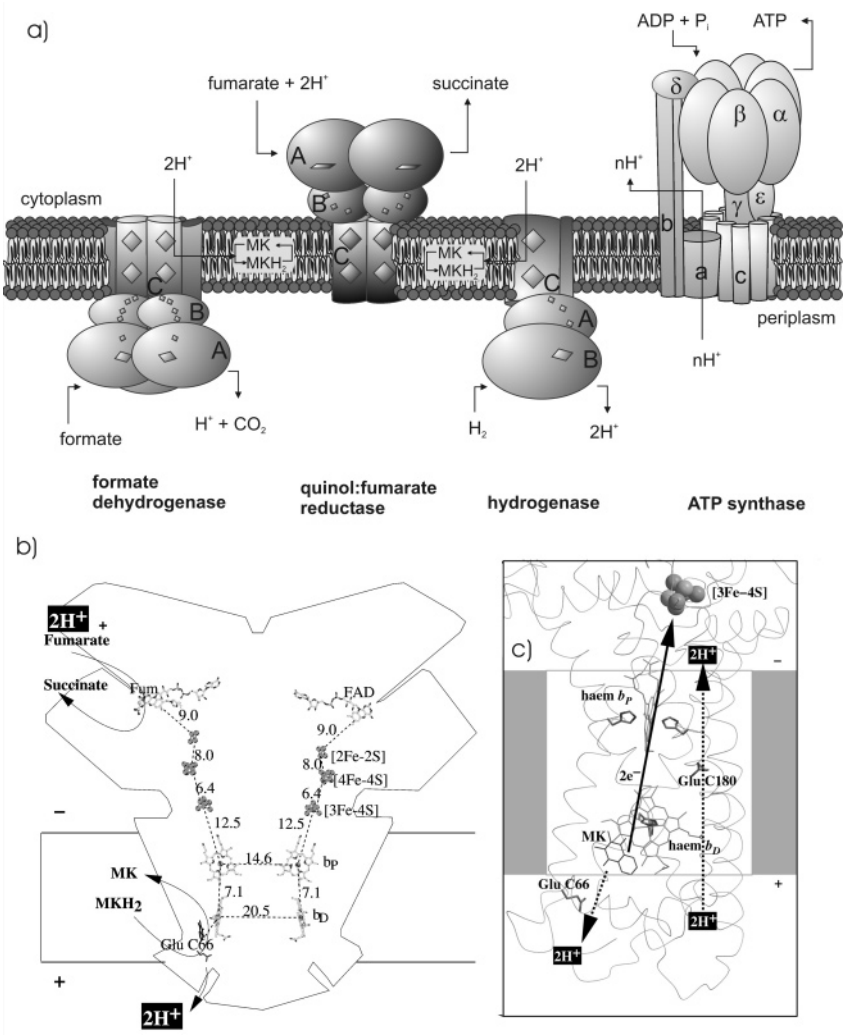

FIGURE 1: Electron and proton transfer in fumarate respiration (a) and *W. succinogenes* QFR (b and c). Positive and negative sides of the membrane are the periplasm and cytoplasm, respectively. (b) Hypothetical transmembrane electrochemical potential generation as suggested by the essential role of Glu C66 for menaquinol oxidation by *W. succinogenes* QFR (*9*). The prosthetic groups of the *W. succinogenes* QFR dimer are displayed (coordinate set 1QLA; *7*). Distances between prosthetic groups are edge−edge distances in angstroms as defined by Page et al. (*48*). Also indicated are the side chain of Glu C66 and a tentative model of menaquinol (MKH_2) binding. The position of bound fumarate (Fum) is taken from PDB entry 1QLB (*7*). (c) Hypothetical cotransfer of one H^+ per electron across the membrane ("E-pathway hypothesis"). The two protons that are liberated upon oxidation of menaquinol (MKH_2) are released to the periplasm (bottom) via the residue Glu C66. In compensation, coupled to electron transfer via the two heme groups, protons are transferred from the periplasm via the ring C propionate of the distal heme b_D and the residue Glu C180 to the cytoplasm (top), where they replace those protons that are bound during fumarate reduction. In the oxidized state of the enzyme, the "E-pathway" is blocked.

from *W. succinogenes* is not directly associated with the generation of a transmembrane electrochemical proton potential (*4*−*6*), the three-dimensional structure of this membrane protein complex, initially solved at 2.2 Å resolution (*7*), revealed locations of the active sites of fumarate reduction (*8*) and menaquinol oxidation (*9*) that are oriented toward opposite sides of the membrane (Figure 1b). Because the binding of two protons upon fumarate reduction invariably occurs from the cytoplasm and the release of two protons associated with menaquinol oxidation invariably occurs to the periplasm, this arrangement of catalytic sites indicated that menaquinol oxidation by fumarate, as catalyzed by *W. succinogenes* QFR, should be associated directly with the establishment of an electrochemical proton potential across the membrane. To reconcile these apparently conflicting experimental observations, the so-called "E-pathway hypothesis" (*10*) has been proposed (Figure 1c). According to this hypothesis, the transfer of two electrons via the two QFR heme groups is strictly coupled to a compensatory, parallel transfer of two protons across the membrane via a proton transfer pathway that is transiently open during the reduction of the two hemes and closed in the oxidized state of the enzyme. The two most prominent constituents of the proposed pathway were suggested to be the ring C propionate of the distal heme b_D and amino acid residue Glu C180. The role of Glu C180 in this context is supported by three previous reports involving a combination of site-directed mutagenesis and structural and functional characterization of the enzyme (*11*) as well as electrochemically induced Fourier transform infrared (FTIR) difference spectroscopy (*12*) and electrostatic calculations (*13*).

It is the aim of this study to clarify any possible heme propionate involvement in the coupling of transmembrane electron and proton transfer as it has been suggested for *W. succinogenes* QFR in the context of the E-pathway hypothesis. The orientation of the ring C propionate of heme b_D in

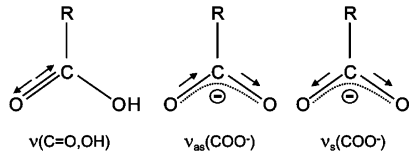

FIGURE 2: Schematic view of the three relevant heme propionate vibrations. On the left, the carbonyl stretching vibration of the protonated carboxyl group (which absorbs between approximately 1700 and 1665 cm^{-1}) is shown; in the middle, the antisymmetric vibration of the deprotonated form (between 1620 and 1540 cm^{-1}); and on the right, the corresponding symmetric vibration (between 1420 and 1300 cm^{-1}). The arrows indicate the motion of the individual atoms. All shown vibrations are sensitive to the ^{13}C isotope exchange, and a maximal downshift of 30−40 wavenumbers upon isotopic labeling of the heme propionate group is expected (*14*, *15*).

the structure of QFR (*7*), together with the results from electrostatic calculations concerning its protonation state (*13*), indicated that this propionate might act as a proton donor/acceptor in the proposed "E-pathway".

In principle, electrochemically induced FTIR difference spectroscopy is the appropriate method to detect reaction-induced protonation and/or environmental changes of the heme propionates experimentally. The C═O stretching modes of protonated heme propionates (Figure 2) are expected to appear in the spectral range from 1700 to 1665 cm^{-1} (*14*, *15*). Contributions from antisymmetric and symmetric COO^- stretching modes of the corresponding deprotonated carboxyl groups can be localized at approximately 1620 to 1540 cm^{-1} and 1420 to 1300 cm^{-1}, respectively (*14*, *15*). However, unlike amino acid side chains, whose role can be investigated by site-directed mutagenesis (*11*, *12*), assignment of potential signals arising from heme propionates requires a different approach, such as selective ^{13}C isotope labeling at the carboxy carbon positions of the heme propionates, which is expected to result in a maximal downshift of 30−40 wavenumbers (cm^{-1}) in the FTIR difference spectra upon isotopic labeling (*14*, *15*). The observed downshift for a C═O vibration might however be smaller if it is coupled to the rest of the molecule, and it is not possible to predict the exact position of the respective signal of the labeled group in the spectrum (*14*). As described below, this labeling procedure involved disrupting heme biosynthesis and supplying a suitably labeled heme precursor.

The first committed precursor in the tetrapyrrole biosynthetic pathway is 5-aminolevulinic acid (ALA), and two different routes for ALA biosynthesis are found in nature (*16*). In the α group of the proteobacteria, in yeast and in mammalian cells, this aminoketo acid is synthesized by a one-step condensation of succinyl−coenzyme A and glycine along the "Shemin" route mediated by the *hemA* gene, encoding for the ALA synthase. However, in higher plants, algae, and many prokaryotic systems, ALA is synthesized from the intact carbon skeleton of glutamate using the C-5 pathway (*17*). This pathway involves an unusual activation of the carboxyl group by formation of Glu-$tRNA^{Glu}$ for the subsequent reduction to glutamate-1-semialdehyde. In a third step, 5-aminolevulinate is formed by an "internal transaminase reaction", which shifts the amino group from the C-1 to the C-2 position. This reaction is catalyzed by the glutamate-1-semialdehyde 2,1-amino-mutase, which is encoded by the *hemL* gene. In the genome sequence of *W. succinogenes* (*18*), the *hemL* gene of the C-5 pathway is

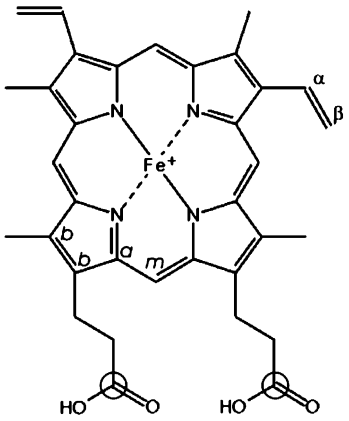

FIGURE 3: Chemical structure of the heme *b* group. The circles indicate the positions of the introduced ^{13}C atoms in the labeled hemes. In addition, the indices of the heme−carbon atoms in the porphyrin ring system and in the vinyl substituents are shown, because they will be used in the following text.

readily identified, but there is no evidence for a *hemA* gene of the "Shemin route". For the construction of the deficient mutant, it was therefore sufficient to disrupt the *hemL* gene of *W. succinogenes*, resulting in an ALA auxotrophy. If [1-^{13}C]-ALA is supplied externally as a heme precursor, the heme propionates of both hemes are labeled at the carboxyl carbon positions, with no ^{13}C enrichment at any other site as shown in Figure 3.

The combined approach of ^{13}C heme propionate labeling and electrochemically induced FTIR difference spectroscopy has previously been successfully employed to investigate the role of heme propionates in *Paracoccus denitrificans* cytochrome *c* oxidase (*14*). However, this approach involved disruption of the *hemA* gene of the "Shemin route" rather than the disruption of the *hemL* gene of the C-5 pathway as performed in the work described here.

Here, we present first experimental evidence directly linking a change in heme propionate protonation and/or conformation to a change in the oxidation state of the low-potential heme b_D of the *W. succinogenes* QFR.

EXPERIMENTAL PROCEDURES

Biological Materials. The quinol:fumarate reductase (QFR) was purified from the laboratory wild-type strain DSM 1740 of *W. succinogenes* (genome accession number EMBL BX571656). Primers were purchased from ThermoHybaid (Ulm, Germany). Taq long-template polymerase for PCR was purchased from Roche (Mannheim, Germany). Restriction and modification enzymes were obtained from Fermentas (St. Leon-Rot, Germany). All cloning steps were performed in *Escherichia coli* JM110 and XL1-blue MRF′ Kan supercompetent cells (Stratagene, La Jolla, CA).

Media and Growth Conditions. *W. succinogenes* was grown in minimal or rich medium (addition to the minimal medium of Brain Heart Infusion, Difco) with formate (electron donor) and fumarate or nitrate (electron acceptors) as described elsewhere (*19*, *20*). The ALA hydrochloride was purchased from Fluka. The [1-^{13}C]-ALA hydrochloride was of 99% purity and was produced by C/D/N Isotopes, Pointe Claire, Quebec, Canada, and purchased from Dr. Ehrenstorfer GmbH, Augsburg, Germany. Kanamycin (GERBU Biochemicals Mart, Gaiberg, Germany) at a concentration of 50 mg/L for *E. coli* or 25 mg/L for *W. succinogenes* was

Table 1: Oligonucleotide Primers Used for PCR Amplification of the *hemL* Gene and the Kanamycin Resistance Cassette

HemL1_Fw	5′-CCG GAT CCG CAT CAC CCC CGA AGC CTT GGC TGT C-3′
HemL1_Rv	5′-CCG AAT TCG GTT AAA CGC CCA AAG TGC CAC GCC C-3′
KanM_Fw	5′-CCC CGG GCC CGG AAA GCC ACG TTG TGT CTC AAA ATC TC-3′
KanM_Rv	5′-CCC CCC ATG GGG CGC TGA GGT CTG CCT CGT GAA GAA GG-3′

added when required. Large-scale protein production is performed in 60 L of anaerobic minimal medium containing 0.2 mM labeled ALA and kanamycin.

DNA Isolation and Manipulation. Plasmid extractions from *E. coli* and DNA extraction from agarose gels were carried out using Qiagen kits (Qiagen GmbH, Hilden, Germany). Other DNA manipulations were performed using standard protocols, as described by Sambrook et al. (*21*). Genomic DNA preparation from *W. succinogenes* was performed using DNeasy Tissue Kit (Qiagen). Construction of pBRΔH01, a plasmid suitable for homologous reciprocal recombination with the genome of *W. succinogenes* (one-step gene disruption), consisted of two stages. In a first stage, the gene glutamate-1-semialdehyde 2,1-aminomutase (*hemL*), including 570 bp from the upstream region and 360 bp from the downstream region, was amplified by PCR from wild-type strain genomic DNA. The amplification was carried out using the two synthesized oligonucleotide primers HemL1_Fw and HemL1_Rv (see Table 1). At the 5′ ends of these primers, the restriction sites *Eco*RI and *Bam*HI were introduced for insertion of the fragment into the vector pBR322 by ligation. In a second stage, this new recombinant plasmid (pBRH01) was then digested with *Nco*I and *Bsp*120I, generating a deletion into the 1.3 kbp *hemL* gene of 740 bp. A 1.21 kbp DNA fragment containing the kanamycin resistance cassette was amplified by PCR using two newly synthesized primers (KanM_Fw and KanM_Rv, see Table 1) flanked by the *Bsp*120I and *Nco*I restriction sites. This latter amplified DNA fragment was inserted into the Δ*hemL* deletion plasmid, maintaining the same direction of the *hemL* promoter. Restriction analysis on this new plasmid, called pBRΔH01, was performed with the four cloning restriction enzymes and *Bss*SI to ensure the correct insertions and directions in the construct. The pBRΔH01 was digested with *Bam*HI/*Eco*RI restriction enzymes, so that only the Δ*hemL* flanking regions, which are needed for double homologous recombination, and the kanamycin resistance gene could be integrated by electroporation into the genome of the wild-type DSM1740 of *W. succinogenes* as described (*22*). As expected, the excised recombinant DNA fragment was about 500 bp larger than the one contained in pBRH01. Recombinant cells were collected from rich medium agar plates containing kanamycin (25 mg/L) and 1 mM ALA. To verify a homologous recombination event, the primers for *hemL* amplification were used to perform a PCR on the isolated colonies. As anticipated, the recombinant genome from the deletion mutant yields an amplified DNA fragment that was unequivocally 500 bp larger than the wild type. The presence of only the target amplified DNA band could rule out the possibility of a nonhomologous recombination mutant, which would be characterized by DNA amplification of both sizes.

Characterization of the Mutant. Of 12 colonies screened, 10 showed the correct *hemL* deletion. The growth yield and doubling times of these 10 mutants were determined by following growth curves in minimal medium containing 1 mM ALA. The deletion strains were also inoculated in rich and minimal media containing kanamycin and different concentrations of ALA. Observation of the cells at the late exponential phase by an optical microscope (400×) did not show any optical difference between the mutant and wild-type cells. In rich medium, growth was obtained in every circumstance, although the final cell density decreased toward a lower concentration of ALA. In minimal medium, growth was experienced only in media containing ALA at a concentration equal to or above 0.2 mM. At the lowest concentration of ALA, we found that several cultures failed to start growing; thus, cell growth was irreproducible, especially upon up-scaling to larger culture volumes. This problem was overcome by increasing the ratio of inoculum to fresh medium from 1:200 to 1:50, so that growth was fully recovered and comparable to higher concentrations of ALA. Because it was observed that longer degassing times of the medium often reduced the irreproducibility of growth, this problem might be due to hypersensitivity of the mutant cells to oxygen. A speculative explanation to the phenomenon could be that the cells may require readily available heme groups and functional heme proteins to eliminate oxygen or reactive oxygen species (ROS) present in the medium before commencing growth.

Expression and Purification. The mutant strain of *W. succinogenes* lacking the *hemL* gene was pre-inoculated overnight in a minimal medium preculture supplemented with 0.4 mM labeled ALA. This was subsequently re-inoculated in the 60 L of minimal medium at a ratio of 1:50. Because of the high cost of the labeled compound, the growth medium was supplemented with ALA at a concentration of 0.2 mM. Cells were harvested by centrifugation at a late exponential phase after 24 to 30 h. The large-scale preparation yielded about 64 g of cells, hence about half of the usual yield for the wild-type strain in rich medium. QFR isolation was performed with identical procedures as described for the wild-type enzyme (*23*), with the exception that the diethylaminoethyl (DEAE) CL-6B was replaced by a DEAE-sepharose chromatography and that the elution gradient was 0−300 mM NaCl. The washing cycles were performed in Centrisart I filtration tubes (Sartorius, Göttingen, Germany) with a cutoff weight of 100 kD and a volume of 2.5 mL. Samples of ^{13}C-labeled and unlabeled QFR were characterized after the isoelectric focusing purification step. The purification profile (see Table S1 in the Supporting Information) based on methylene blue (MB) activity exhibits a usual enzymatic behavior of the QFR. Analysis by sodium dodecyl sulfate−polyacrylamide gel electrophoresis (SDS−PAGE) of the isoelectric focusing (IEF)-purified QFR yielded the three characteristic bands of the three subunits A, B, and C and very weak contaminant bands, comparable to typical wild-type QFR preparations (see Figure S1 in the Supporting Information). The heme *b* concentration was also calculated spectrophotometrically at the Soret band and proved a molar heme/protein ratio of about 2:1. Further proof is given by the observation of two titrating groups of equal contributions in the heme redox titration curve, as expected for a di-heme-

containing QFR (see Figure S3 in the Supporting Information). The samples subjected to FTIR spectroscopy analysis were washed and concentrated in 100 mM potassium phosphate (KP_i) buffer at pH 7 containing 100 mM KCl as the supporting electrolyte and 1 mM *n*-dodecyl-β-D-maltoside (Glycon Biochemicals, Luckenwalde, Germany) [cmc = 0.17 mM (*24*)] as the detergent. Samples with protein concentrations of about 1.5 mM were prepared for the FTIR-spectroscopic experiments. The final sample concentration was adjusted in Vivaspin 500 μL concentrators (Vivascience, Hannover, Germany) with a 100-kD cutoff. The total protein concentration was measured by the bicinchoninic acid assay (BCA assay, Pierce Biotechnology, Bonn, Germany) (*25*), and the heme *b* concentration was determined photometrically as described earlier (*9*, *26*).

Enzymatic Activities. The ^{13}C-labeled QFR preparation obtained after IEF was diluted to a concentration of about 1 mg/mL in a buffer containing 20 mM HEPES, 1 mM EDTA, 2 mM malonate, 0.01% dodecyl-β-D-maltoside, and 0.1% decyl-β-D-maltoside and kept at 37 °C for 30 min prior to the assay. Two kinds of assays were performed. First, the reduction of MB by succinate was monitored ("MB assay"; *27*, *28*). This assay requires only the hydrophilic QFR subunits A and B. Second, the oxidation of 2,3-dimethyl-1,4-naphthoquinol ($DMNH_2$) by fumarate was monitored ("$DMNH_2$ assay"; *23*, 29) This assay requires all three QFR subunits A, B, and C. The specific activities of the purified ^{13}C-labeled protein, determined with the "MB assay" (17.4 units/mg) and the "$DMNH_2$ assay" (6 units/mg), are perfectly comparable to those of the unlabeled wild-type QFR enzyme (*9*).

Native Quinone Quantification. As already described in the literature [e.g., for the photosynthetic reaction center (*30*)], hydrophobic substrates such as quinones, which bind to the transmembrane region of the enzyme, are found to substoichiometrically copurify during the isolation procedure. Quinones give rise to characteristic IR signals at certain wavelengths during redox changes around −70 mV (all quoted potentials versus the standard hydrogen electrode, SHE) that may be interfering with our FTIR spectra analysis. To exclude any significant influence because of major quinone-occupancy differences between QFR preparations with unlabeled and ^{13}C-labeled heme propionates, quinone-like species (methyl-menaquinone and menaquinone) were extracted from the same protein samples used for FTIR spectroscopy. Quantification of native quinone was performed as described earlier (*31*) using commercially available (Sigma, Munich, Germany) menaquinone MK_4 ($VitK_2$) as a standard. Separation and quantification were carried out by HPLC, giving a "quinone/monomer" ratio of 0.23 ± 0.03.

MALDI−TOF Analysis of Hemes. A volume of 50 μL from the purified ^{13}C-labeled and unlabeled QFR at a concentration of about 20 mg/mL was used for heme extraction with a procedure already described (*32*). After solvent evaporation, the extracted hemes were redissolved in 50 μL of acetonitrile and stored at −20 °C until mass spectrometer measurements. A Voyager DE-PRO (Applied Biosystems, Framingham, MA) mass spectrometer and 2,5 DHB matrix (20 mg/mL dihydroxybenzoic acid in 0.1% TFA in 3:1 water/ACN) were used. Mass spectra were recorded in positive-reflector mode with external calibration. Each spectrum is accumulated over 20−30 laser shots. Measurements of the hemes extracted from the unlabeled and ^{13}C-labeled samples yielded clear signals at 616 atomic mass units (*m*/*z*) and 618 atomic mass units (*m*/*z*), respectively (see Figure S2 in the Supporting Information). Examination of all of the peaks obtained from the labeled sample demonstrated that only a negligible percentage of the propionates were not isotopically labeled.

Electrochemistry, FTIR, and Vis Spectroscopy. Electrochemically induced FTIR difference spectroscopy and heme titration were performed in an ultrathin-layer spectroelectrochemical cell (*33*). The preparation of the samples as well as the experimental setup (i.e., electrochemistry and spectrometer) and conditions (i.e., surface modification of the gold grid working electrode, 15 redox mediator substances of ∼40 μM each, sample volume, equilibration times, and data acquisition and processing) were the same as described previously in refs *9* and *12*. All measurements were performed at 5 °C. For details regarding the determination of the midpoint potentials of the heme *b* groups of QFR, see ref *9*. The midpoint potentials of the ^{13}C-labeled heme *b* groups of QFR were determined at pH 7 by monitoring the absorption changes of the Soret and α bands of the hemes in the visible spectral range during a potential titration. The observed midpoint potentials for the high- and low-potential hemes were +4 and −137 mV, respectively (the corresponding titration curves are shown in Figure S3 in the Supporting Information). The respective values for the unlabeled QFR WT were −9 and −152 mV (*9*) Thus, both values are approximately 10−15 mV more positive than the average midpoints measured for the unlabeled WT. For the latter, the statistical basis was broader because more independent data could be collected, and a typical experimental error of ±10 mV was estimated from the data scattering at pH 7. For the ^{13}C-labeled enzyme, the value obtained for the high-potential proximal heme b_P lied within this error and the value for the low-potential distal heme b_D exceeded it by +5 mV. Hence, the influence of the ^{13}C label on the heme midpoint potentials, if any, was minor. We concluded that this difference was due to experimental errors rather than a real shift of the midpoints.

All IR difference spectra in the range of 1800−1000 cm^{-1} were recorded using a modified Bruker IFS 25 FTIR spectrometer that has been described in previous reports (*34*, *35*). Difference spectra were obtained by applying an initial potential at which a reference spectrum was recorded. Then, the electrode potential was changed and another single-beam spectrum was recorded after equilibration of the sample. Because of the presence of redox mediators, the very thin layer of protein solution, and the gold grid surface modification, equilibration times were rather short (of the order of minutes). None of the presented data was smoothed or subjected to any spectral deconvolution. The single method employed to enhance the signal-to-noise ratio was to average multiple single-beam spectra (each being the average of 128 interferograms with a spectral resolution of 4 wavenumbers, a triangular apodization function, and a zero-filling factor of 2) that were recorded at the same electrode potential. Because of the small amplitude of the signals that were investigated and because of the occurrence of noticeable baseline instabilities in the same experiments (cf. Figures 5 and 6), the spectra corresponding to the "partial-potential steps" had to be baseline-corrected: the respective pairs of

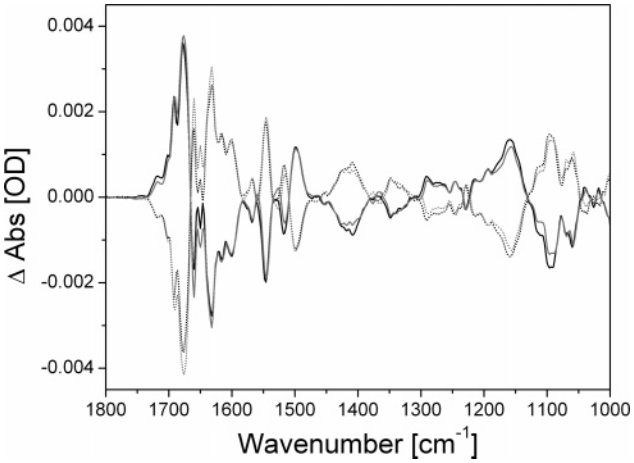

FIGURE 4: Electrochemically induced FTIR difference spectra of unlabeled and ^{13}C-labeled QFR at pH 7, "full-potential step". A comparison of reversible "oxidized-minus-reduced" (—) and "reduced-minus-oxidized" (···) FTIR difference spectra of unlabeled (in black, average of 23 datasets) and ^{13}C-labeled (in gray, average of 34 datasets) QFR. The reference electrode potentials (versus SHE′) for the spectra displayed were +0.21 V (full oxidative potential) and −0.37 V (full reductive potential).

difference spectra, e.g., "reduced-minus-intermediate" and "intermediate-minus-reduced", were summed to determine the baseline drift, which was subsequently subtracted. As a consequence of the correction, the opposite directions, e.g., "reduced-minus-intermediate" and "intermediate-minus-reduced", are symmetrical and contain the same information; thus, only one direction is shown in Figures 5 and 6. However, also, the reactions that involved the intermediate potential were reversible as observed for the full-potential step. The data shown in Figure 4 was not subjected to a baseline correction.

RESULTS AND DISCUSSION

In anaerobic bacteria, the glutamate-1-semialdehyde-2,1-amino-mutase encoded by the *hemL* gene is responsible for the synthesis of ALA, a precursor of the heme biosynthesis (*36*). The deletion of the *hemL* gene in the wild-type *W. succinogenes* resulted in an auxotrophic strain that did not possess a functional glutamate-1-semialdehyde-2,1-amino-mutase and was therefore able to grow in minimal medium only by making use of exogenously supplied ALA. After the [1-^{13}C]-ALA was provided, the *hemL*-deletion mutant strain of *W. succinogenes* was able to produce a QFR specifically and highly ^{13}C-labeled at the carboxyl carbon atoms of the heme propionates. After protein expression and purification, the labeled QFR sample was characterized and compared to the unlabeled sample to exclude any difference in the physicochemical properties between the two samples. Analysis by MALDI−TOF (see Figure S2 in the Supporting Information) ascertained that full labeling of the heme propionates indeed occurred, thus confirming the results of the genetic work and providing a solid basis for the discussion of the spectroscopic results. Enzymatic activities of the ^{13}C-labeled QFR were very similar to those of the unlabeled QFR, ensuring that the former enzyme is correctly folded and functional (see the Experimental Procedures). Because both hemes are believed to be involved in the total enzymatic activity (*9*), the full functionality indicates that the QFR contains all cofactors, including the labeled hemes (see also the Experimental Procedures). The high specific activity together with the analysis by SDS−PAGE (see Figure S1 in the Supporting Information) of the isolated labeled QFR after isoelectric focusing allowed the conclusion that the enzyme functionality and purity is comparable to the usual wild-type QFR preparation. Furthermore, the redox midpoint potentials of the labeled QFR hemes have been measured by visible spectroscopy (see Figure S3 in the Supporting Information). Any differences were found to be insignificant within the context of this paper.

Reversible FTIR Difference Spectra of the "Full-Potential" Step. Figure 4 shows the reversible electrochemically induced FTIR difference spectra of the unlabeled and ^{13}C-labeled QFR enzymes, respectively, at pH 7 for the "full-potential" step, i.e., with an initial reference potential at which all cofactors were fully reduced and a final potential at which all were fully oxidized (and vice versa). The FTIR difference spectra obtained for the QFR containing the ^{13}C-labeled heme propionates were very similar to those for the unlabeled QFR, which were discussed in ref *12*. This indicated that the possible heme propionate contributions in the full-potential step were of small amplitude. Thus, it was advisable to experimentally separate the contributions of the individual heme groups and to compute double-difference spectra to better resolve any smaller signals (see below).

Signals of Hemes and Heme Propionates. A multitude of heme vibrations, which partly overlap with the amide I, II, and III regions, have been observed and assigned in many FTIR and Raman studies for the heme porphyrin ring, substituents, and propionates (e.g., see refs *14* and *37*−*41*). Also in the case of QFR, the two heme *b* groups are expected to show significant contributions to the FTIR difference spectra, which reflect the electrochemically induced redox-state changes of the hemes. Protonated heme propionates are generally expected to contribute between 1700 and 1665 cm^{-1} (*14*, *15*). This region overlaps with the amide I vibrations and is dominated by the large negative difference signal at 1678 cm^{-1} (see Figure 4). Thus, it is difficult to assign contributions of any protonated heme propionates without further distinction such as ^{13}C-labeling (as performed for this study). The deprotonated forms of the propionates exhibit antisymmetric $\nu_{as}(COO^-)$ (between 1620 and 1540 cm^{-1}) and symmetric $\nu_s(COO^-)$ vibrations (between 1420 and 1300 cm^{-1}) (*14*, *15*). Furthermore, assignments of heme propionate bands are complicated because ionized Asp or Glu side-chain contributions are expected at comparable frequencies (*37*).

The strong absorbance at 1545 cm^{-1} in ^1H_2O in the reduced state (see Figure 4) is tentatively assigned to $\nu(C_bC_b)$ and/or antisymmetric $\nu_{as}(C_aC_m)$ porphyrin modes of the heme *b* groups (*38*, *39*); the labeling of heme *b* atoms is analogous to ref *39*. However, the band did not shift upon deuteration (*12*), as would be expected for this assignment (*39*). A corresponding symmetric mode to $\nu_{as}(C_aC_m)$, namely, $\nu_s(C_aC_m)$, is expected between 1486 and 1458 cm^{-1} (*38*, *39*). The reduced-minus-oxidized difference spectrum of the QFR enzyme featured a small signal in the oxidized state at 1462 cm^{-1} in ^1H_2O.

The $\nu(C_aC_b)$ vibration is expected in an adjacent frequency region between 1450 and 1435 cm^{-1} (*40*). In the respective range in the QFR difference spectrum, a small shoulder is present in the reduced state around 1438 cm^{-1}.

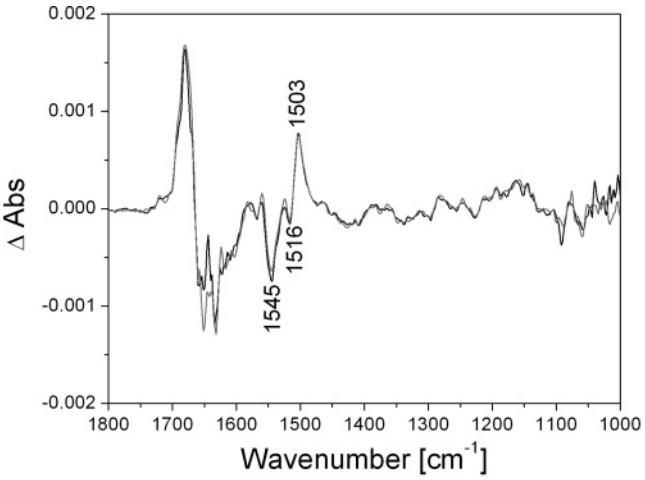

FIGURE 5: Electrochemically induced FTIR difference spectra of unlabeled and ^{13}C-labeled QFR at pH 7, "high-potential step". A comparison of "oxidized-minus-intermediate" FTIR difference spectra of unlabeled (in black, average of 12 datasets) and ^{13}C-labeled (in gray, average of 11 datasets) QFR. The reference electrode potentials for the spectra displayed were +0.21 V (full oxidative potential) and −0.08 V (intermediate potential).

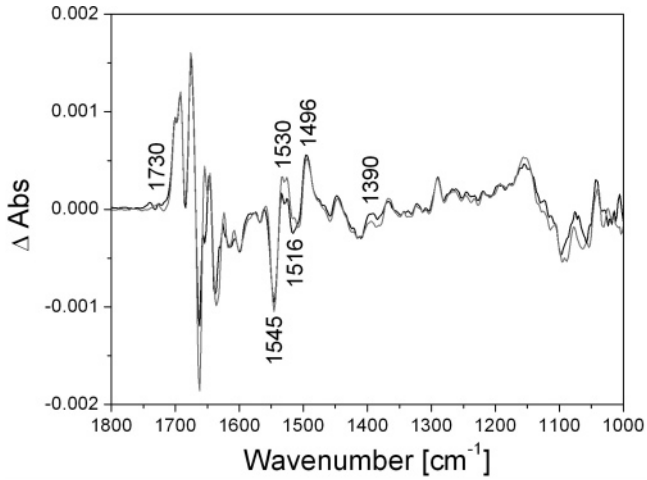

FIGURE 6: Electrochemically induced FTIR difference spectra of unlabeled and ^{13}C-labeled QFR at pH 7, "low-potential step". A comparison of "intermediate-minus-reduced" FTIR difference spectra of unlabeled (in black, average of 19 datasets) and ^{13}C-labeled (in gray, average of 22 datasets) QFR. The reference electrode potentials for the spectra displayed were −0.08 V (intermediate potential) and −0.37 V (full reductive potential).

Below 1400 cm^{-1}, two further significant heme porphyrin vibrations are expected, the $\nu(C_aN)$ vibration between 1390 and 1320 cm^{-1} (*40*) and the $\delta(C_mH)$ mode between 1270 and 1150 cm^{-1} (*39*). The QFR difference spectra exhibit small contributions in the oxidized state between 1390 and 1358 cm^{-1} and in the reduced state between 1356 and 1312 cm^{-1}. Also the region below 1270 cm^{-1} shows several bands belonging to either the reduced or oxidized state. However, all contributions below 1400 cm^{-1} are altered upon deuteration (data not shown). Thus, an assignment to the respective heme vibrations is by no means unequivocal, and additional non-heme vibrations such as amide III, FAD, quinone, and several amino acid vibrations also have to be considered. Finally, signals from the heme substituents are expected: the positive band at 1617 cm^{-1} (see Figure 4) might be assigned to a heme vinyl $\nu(C_\alpha{=}C_\beta)$ stretching vibration in the reduced state (*39*, *41*).

Separation of Redox-Induced IR Signals from Hemes b_D and b_P. The locations of the high- and low-potential heme groups in the structure of *W. succinogenes* QFR have previously been assigned to the proximal and distal heme positions, respectively (*13*). Because the midpoint potentials of these two heme groups differ by almost 150 mV, it is feasible to separate the corresponding spectral signals and address the low- and high-potential hemes individually by setting the appropriate reference potentials in the experiment. The best separation is achieved at an "intermediate" potential, which is equal to the average of the two midpoints. At this intermediate electrode potential of −0.08 V, about 95% of the high-potential heme groups are reduced and 95% of the low-potential hemes are oxidized. Thus, the separation of the two heme midpoint potentials is wide enough to guarantee negligible contributions (≤5%) of the respective other heme in the two partial-potential steps "oxidized-minus-intermediate" and "intermediate-minus-reduced" (and vice versa). The corresponding spectra are shown in Figures 5 and 6. Even without inspection of double-difference spectra, the differences between the unlabeled and ^{13}C-labeled QFR were clearly more pronounced for the low-potential partial step. The positions of the spectral differences are indicated in Figure 6 between 1530 and 1516 cm^{-1} and around 1390 cm^{-1}, and the marked regions coincided very well with the expected frequency ranges for vibrations of protonated and deprotonated heme propionates (*14*, *15*).

Furthermore, it was possible to add the difference spectra of the two different partial-potential steps to obtain a computed difference spectrum of the full-potential step (see Figure S4 in the Supporting Information). The close similarity of the computed and measured difference spectra verified the approach of subdividing the complete redox reaction into two halves. The discrepancies between the computed and original difference spectra of the full-potential step might arise because of conformational changes or environmental differences, which are specifically related to the intermediate potential state, because this state does not contribute to the full-potential step. This addition of difference spectra was performed in an equal manner for the ^{13}C-labeled enzyme (data not shown).

FTIR Difference Spectra of the "Partial-Potential" Steps. The FTIR difference spectra of the two partial-potential steps, which include the intermediate potential, reflect the redox transitions of the two heme groups b_D and b_P, but spectral contributions from other cofactors, prosthetic groups, and the protein itself are inevitable. Positive signals in Figure 5 belong to the oxidized state, and negative signals belong to the intermediate state. In Figure 6, positive signals refer to the intermediate state, whereas negative signals are associated with the reduced state. Although the difference spectra of the two different partial steps reveal clear deviations, the positions and proportions of the main spectral features are similar for both partial-potential steps and also comparable for the unlabeled and ^{13}C-labeled QFR enzyme (see Figures 5 and 6), except for the deviations mentioned above that are related to the ^{13}C label. The strong differences between the two steps in the amide I range (∼1700−1610 cm^{-1}) of the spectra could arise from distinct sets of amino acid residues, which are only addressed in the course of the individual potential step, and/or they could indicate redox-induced

structural changes of the polypeptide backbone of QFR, which are either related to the redox transition of the high- or low-potential heme.

As stated above, the sharp peak at 1545 cm^{-1}, which is observed in the full-potential step, is tentatively assigned to heme porphyrin $\nu(C_bC_b)$ and/or $\nu_{as}(C_aC_m)$ vibrations (*12*). An analogous signal is present in both partial-potential steps (with lower intensity compared to the full-potential step), which is in line with this assignment. The contributions observed at 1516 and 1501 cm^{-1} in the full-potential step, which were tentatively assigned to Tyr modes (*12*), are also visible in the high-potential partial step at 1516 and 1503 cm^{-1} and at 1516 and 1496 cm^{-1}, in the low-potential step. If the performed tentative assignment for the respective IR bands is correct, this observation would indicate the (de)-protonation reaction of two different Tyr residues or that a single Tyr is engaged in a very broad transition with respect to the applied redox potential. Numerous Tyr residues in *W. succinogenes* QFR (38 Tyr/QFR monomer) are conceivable as possible candidates for involvement in the induced redox reaction. Alternatively, the pair of bands might however have to be assigned to heme vibrations. Further mutagenesis work is required to clarify the precise origin of this distinct spectral feature.

As mentioned in previous studies, the PO modes from the potassium phosphate buffer below 1200 cm^{-1} reflect proton exchange of the enzyme and the mediators with the buffer (*42*−*44*). The spectra for the two partial-potential steps show that this effect is more pronounced in the low-potential partial step (see Figures 5 and 6) because the amplitude of the respective bands is stronger in this step. A quantification and further assignment of the observed PO buffer bands to a particular protonation reaction was not attempted because signals of comparable amplitudes in the range between 1200 and 1000 cm^{-1} can also be observed in experiments lacking the protein (data not shown). For the bc_1 complex, such quantification was performed in ref *44*.

Although the QFR samples contained some native quinone species, there were no noticeable contributions to the FTIR difference spectra (*12*). The same holds true for the possible discrepancy in quinone content in the labeled and unlabeled QFR samples and the corresponding double-difference spectra because no clearly quinone-like signals could be detected. What could be identified while addressing the question of potential quinone contributions was an artifact at 1292 cm^{-1} in the "intermediate-minus-reduced" difference spectra (see Figure 6). With the help of control experiments, this feature could be ascribed to the mediators that were too highly concentrated in this particular experiment. This signal might well originate from one or several quinones (*45*, *46*) in the mediator mixture, but as verified by measuring the mediator−buffer mixture alone (data not shown), the position of this band does not interfere with the intended assignments of heme propionate signals. Especially the range above 1500 cm^{-1}, where the most prominent and reliable heme propionate difference signals were identified, is free from any possible quinone contributions (*45*, *46*). Most importantly, the FTIR double-difference spectra of the labeled and unlabeled QFR did not display any noticeable signal in the region around 1292 cm^{-1} (Figure 8).

Signals of Protonated Heme b_D Propionates. The range of Asp or Glu ν(COOH) modes above approximately 1710 cm^{-1} (*37*) is of particular interest with respect to a possible coupling of proton transfer via acidic groups to the redox transition of the high- and low-potential heme, respectively. At 1718 cm^{-1}, a signal in the full-potential step of the unlabeled QFR wild-type enzyme has tentatively been assigned to a FAD $\nu(C_4{=}O)$ vibration in the oxidized state (*12*). This signal can also be identified in the oxidized state of the high-potential partial step, and it is slightly more pronounced in the ^{13}C-labeled enzyme (see Figure 5). The affiliation of this signal to the high-potential step is in line with the midpoint potential of the covalently bound FAD in QFR [−20 mV (*47*)]. The difference spectra of the ^{13}C-labeled and unlabeled QFR associated with the low-potential step and thus with heme b_D differ considerably above 1710 cm^{-1} (see Figure 7). In the unlabeled WT, two separated positive contributions associated with the intermediate state are centered at 1740 and 1726 cm^{-1}. In the ^{13}C-labeled enzyme, the low-potential step reveals one broad contribution in the intermediate state around 1728 cm^{-1}. Hence, it has to be concluded that at least one propionate of b_D contributes in this high-frequency range and that the vibration is downshifted by 15 to 20 cm^{-1} upon ^{13}C-labeling (see Figure 7), where they are heavily obscured by other vibrations (i.e., the amide I and the strong water absorbance, which are both centered around 1650 cm^{-1}), which agrees well with the expected range of a possible downshift and with observations from other studies (*14*, *15*). On the basis of observations from multiple independent experiments on the unlabeled QFR WT enzyme, the signal around 1718 cm^{-1} appears to be more susceptible for amplitude variations under identical experimental conditions. Although frequencies above 1710 cm^{-1} would be very high for a ν(COOH) heme propionate vibration (*14*), the results obtained in this study indicate a frequency for a propionate group carboxyl vibration that is in the range of Glu or Asp ν(COOH) modes (*37*). However, this is conceivable if the local environment of the specific propionate is very hydrophobic so that it is not hydrogen-bonded, enabling the observed high frequency for the ν(COOH) mode. If experimental errors such as insufficient equilibration or differences in local pH can be excluded, the

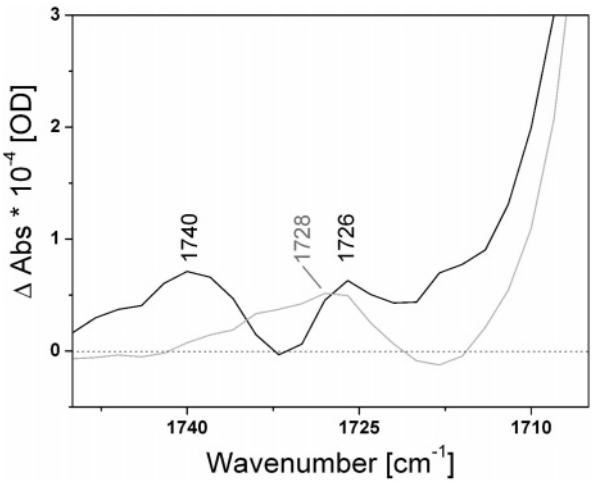

FIGURE 7: Detail of FTIR difference spectra of unlabeled and ^{13}C-labeled QFR at pH 7. FTIR difference spectra of the partial-potential step "intermediate-minus-reduced" (solid black line) for the unlabeled WT and "intermediate-minus-reduced" (solid gray line) for the ^{13}C-labeled WT. The reference electrode potentials are the same as indicated above.

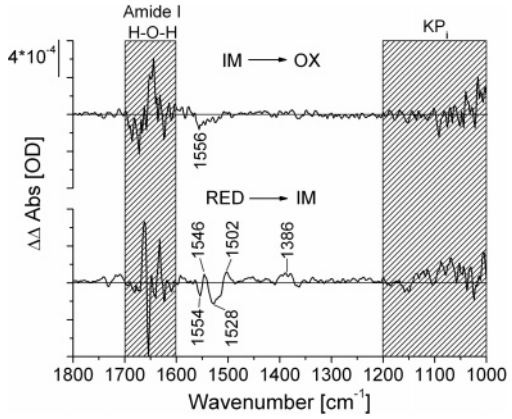

FIGURE 8: FTIR double-difference spectra of "unlabeled-minus-^{13}C-labeled" QFR at pH 7. The upper trace shows the data for the potential step "oxidized-minus-intermediate", whereas the lower shows the data for "intermediate-minus-reduced". The positions of the relevant double-difference bands are indicated in the figure. The crossed areas correspond to regions of elevated noise level (in the amide I region between 1700 and 1600 cm^{-1} because of the strong H_2O and amide I absorbance and below 1200 cm^{-1} because of the absorbance of KP_i-buffer modes), which are difficult to handle in double-difference spectra and should thus be excluded from the analysis.

observed spectral differences between the specifically ^{13}C-labeled and unlabeled QFR in this range are a direct consequence of the ^{13}C-labeling of the heme propionates. Furthermore, such a scenario is covered by the particular position and environment of the ring C propionate of heme b_D because it is oriented parallel to the membrane plane inside the hydrophobic subunit (and not along the membrane normal as the other propionates, see Figure 1b). Thus, it is feasible that the observed difference signals above 1710 cm^{-1} contain heme propionate contributions, which indicates a redox-coupled protonation change and/or an environmental change of the ring C propionate group of b_D. However, it remains difficult to explain the entire spectral features in terms of heme propionate vibrations, and additional effects, e.g., because of small scaling errors, cannot be excluded.

Signals of Anti- and Symmetric Vibrations of Deprotonated Heme b_D Propionate(s). To obtain a clearer picture of the spectral differences that were induced upon ^{13}C-labeling of the heme propionates of QFR, it is possible to compute and analyze "double-difference" spectra (see Figure 8) by subtracting the spectra shown in Figures 5 and 6, respectively. The double-difference spectra are rather noisy, which is almost inevitable because independent experiments always differ slightly from each other. In addition, the spectra have to be scaled for a comparison (*12*), which is another potential source for inaccuracies in the double-difference spectra. Furthermore, the signals that are of interest here are comparatively small. As can be seen in Figure 8, rather large double-difference signals occur in the amide I range between roughly 1700 and 1600 cm^{-1}. Because the ^{13}C label is not expected to affect any amide vibrations directly, it is assumed that the observed signals are related to and/or strongly influenced by an elevated noise level in this region because of the intense H_2O and amide I absorbances, which lead to a reduced detector sensitivity in this frequency range (*14*). Thus, this particular region as well as the range between 1200 and 1000 cm^{-1} should be excluded from the analysis (see also the caption of Figure 8). The good agreement of the difference spectra of unlabeled and labeled QFR for the high- and low-potential partial steps, respectively, demonstrated that the independent procedures of baseline-correcting the FTIR difference spectra in Figures 5 and 6 do not interfere with the spectral information contained in the data, especially not in the range of signals that are related to the anti- and symmetric vibrational modes of the heme propionates.

The direct comparison of the double-difference spectra corresponding to the high- and low-potential partial steps, respectively, clearly allows the assignment of the observed contributions to the redox transition of the low-potential distal heme b_D. As can be seen in Figure 8 for the low-potential step, the positions of the obtained FTIR double-difference bands of "unlabeled-minus-^{13}C-labeled" QFR in the IR spectrum coincide very well with the expected ranges for propionate vibrations (*14*, *15*). The negative band in the FTIR double-difference spectrum of the low-potential step at 1554 cm^{-1} (^{12}COO$^-$) is shifted down to 1546 cm^{-1} (^{13}COO$^-$) by 8 cm^{-1}. The negative band at 1528 cm^{-1} (^{12}COO$^-$) is shifted down to 1502 cm^{-1} (^{13}COO$^-$) by 26 cm^{-1}. Because both signals are negative (in an "intermediate-minus-reduced" spectrum), they belong to the reduced state. Furthermore, both signals indicate a deprotonation and/or an environmental change of at least one of the two propionates of heme b_D upon reduction. As inferred from the crystal structure of QFR (*7*) and rationalized by previous electrostatic calculations (*13*), the ring D propionate of the low-potential distal heme b_D is engaged in a salt bridge with the positively charged Arg C162 and both heme propionates of the high-potential proximal heme b_P are involved in salt bridges with positively charged amino acid residues. This leaves the ring C propionate of heme b_D as the only likely candidate to explain the larger signal at 1528 cm^{-1}. The smaller signal at 1554 cm^{-1} could arise from a slightly altered environment of also the ring C propionate of heme b_D upon reduction, if the (de)-protonation reaction occurs in the vicinity of the p*K* value of the particular propionate group. Thus, the data indicate a deprotonation, probably superimposed by an environmental or conformational change of currently unknown nature, of the ring C propionate of heme b_D upon reduction. The present experiments do not allow an unambiguous identification of the group(s) to which this protonation is transferred, but we cannot rule out that the protonation of the Glu C180 side chain upon heme reduction demonstrated previously (*12*) occurs, at least partially, at the expense of ring C propionate of heme b_D.

Only residual contributions of very small amplitude (as mentioned above, an overlap of 5% at the intermediate potential was estimated for the contributions of the two hemes) plus noise are seen at the corresponding wavenumbers in the "oxidized-minus-intermediate" potential step (Figure 8).

The corresponding mandatory signals for the symmetric ν_s(COO$^-$) vibrations are present in the double-difference spectra in the expected frequency range between 1410 and 1360 cm^{-1}, including the possible downshift upon ^{13}C-labeling (*14*, *15*), although they are less pronounced. At least for the acidic side chains of Asp and Glu, this observation is in line with smaller extinction coefficients for symmetric ν_s(COO$^-$) modes compared to the antisymmetric ones (*37*). Another experimental observation, which supports the assignment of heme propionate vibrations, was to perform the

presented experiments in a D_2O-based buffer (data not shown). The respective FTIR difference spectra clearly show that the assigned propionate signals are sensitive to a $^1H_2O/^2H_2O$ solvent exchange, which is the classical straightforward method to verify the assignment of IR signals of carboxyl groups (e.g., ref *37*).

Differences between the Full- and Partial-Potential Steps for b_D. The direct comparison of the two partial-potential steps (Figures 5 and 6) and the corresponding FTIR double-difference spectra (Figure 8) led to the conclusion that only the propionate(s) of the low-potential heme group b_D are involved in a (de)protonation reaction and/or an environmental change. Thus, it can equally be deduced that the propionate groups of the high-potential heme do not contribute to the FTIR difference spectra of the full-potential step. A close observation of the spectral features above 1700 cm^{-1} shows that there are noticeable differences between the full- and the low-potential step (cf. Figures 4 and 6). The observed discrepancies that are visible for the two steps could be due to the different reference potentials "intermediate" and "oxidized", respectively. At the intermediate potential, the (high-potential) proximal heme b_P is reduced and heme b_D is oxidized. At the oxidizing potential, *both* hemes are fully oxidized. Hence, it is feasible that the redox state of the proximal heme influences the redox transition of the distal heme b_D. In the electrostatic calculations, the two oxidized hemes destabilize each other by 0.6 ΔpK units (*13*), whereas the interactions with and among the reduced heme species are negligible. Thus, on the basis of the presented results and simulations (*13*), it is conceivable that the different redox state of the proximal heme b_P has a noticeable influence (minor frequency shifts and/or intensity variations, as can be seen in Figure 8) on the vibrations of the ionized propionates of the oxidized distal heme b_D.

CONCLUSION

The absence of significant contributions from the propionates of the high-potential proximal heme b_P is in line with the results from both the structure (*7*) and the electrostatic calculations that both propionates are involved in stable salt bridges and consequently not available for redox-driven proton transfer (*13*). For the distal heme b_D, the ring C propionate is concluded to be the dominating source for the observed spectral differences between QFR with unlabeled and ^{13}C-labeled heme propionates, respectively. The interpretation of the obtained experimental data associated with the distal heme b_D and particularly with the ring C propionate, in terms of a (de)protonation event, possibly accompanied by an environmental effect that could well be a conformational change, agrees very well with the suggested role of this propionate in the proposed "E-pathway" hypothesis of coupled transmembrane electron and proton transfer (*10*).

ACKNOWLEDGMENT

The authors are grateful to Prof. Michael Karas and Dr. Ute Bahr from the Institute of Pharmaceutical Chemistry, J. W. Goethe University, Frankfurt am Main, for performing the MALDI−TOF measurements.

SUPPORTING INFORMATION AVAILABLE

(Table S1) Purification table of the ^{13}C-labeled QFR, (Figure S1) SDS−PAGE of ^{13}C-labeled QFR at different purification steps, (Figure S2) MALDI−TOF analysis of the extracted hemes, (Figure S3) heme *b* titration curve of the ^{13}C-labeled QFR wild type at pH 7, and (Figure S4) comparison of FTIR difference spectra of the "full-potential step" as measured to those computed by summation of the spectra of the "low-potential step" and "high-potential step". This material is available free of charge via the Internet at http://pubs.acs.org.

REFERENCES

1. Kröger, A. (1978) Fumarate as terminal acceptor of phosphorylative electron transport, *Biochim. Biophys. Acta 505*, 129−145.
2. Lancaster, C. R. D. (2004) Structure and function of succinate: quinone oxidoreductases and the role of quinol:fumarate reductases in fumarate respiration, in *Respiration in Archaea and Bacteria Volume 1: Diversity of Prokaryotic Electron Transport Carriers* (Zannoni, D., Ed.) pp 57−85, Kluwer Scientific, Dordrecht, The Netherlands.
3. Mitchell, P. (1979) Keilin's respiratory chain concept and its chemiosmotic consequences, *Science 206*, 1148−1159.
4. Geisler, V., Ullmann, R., and Kröger, A. (1994) The direction of the proton exchange associated with the redox reactions of menaquinone during electron transport in *Wolinella succinogenes*, *Biochim. Biophys. Acta 1184*, 219−226.
5. Kröger, A., Biel, S., Simon, J., Gross, R., Unden, G., and Lancaster, C. R. D. (2002) Fumarate respiration of *Wolinella succinogenes*: Enzymology, energetics, and coupling mechanism, *Biochim. Biophys. Acta 1553*, 23−38.
6. Biel, S., Simon, J., Gross, R., Ruiz, T., Ruitenberg, M., and Kröger, A. (2002) Reconstitution of coupled fumarate respiration in liposomes by incorporating the electron transport enzymes isolated from *Wolinella succinogenes*, *Eur. J. Biochem. 269*, 1974−1983.
7. Lancaster, C. R. D., Kröger, A., Auer, M., and Michel, H. (1999) Structure of fumarate reductase from *Wolinella succinogenes* at 2.2 Å resolution, *Nature 402*, 377−385.
8. Lancaster, C. R. D., Gross, R., and Simon, J. (2001) A third crystal form of *Wolinella succinogenes* quinol:fumarate reductase reveals domain closure at the site of fumarate reduction, *Eur. J. Biochem. 268*, 1820−1827.
9. Lancaster, C. R. D., Gross, R., Haas, A., Ritter, M., Mäntele, W., Simon, J., and Kröger, A. (2000) Essential role of Glu-C66 for menaquinol oxidation indicates transmembrane electrochemical potential generation by *Wolinella succinogenes* fumarate reductase, *Proc. Natl. Acad. Sci. U.S.A. 97*, 13051−13056.
10. Lancaster, C. R. D. (2002) *Wolinella succinogenes* quinol:fumarate reductase 2.2 Å resolution crystal structure and the E-pathway hypothesis of coupled transmembrane proton and electron transfer, *Biochim. Biophys. Acta 1565*, 215−231.
11. Lancaster, C. R. D., Sauer, U. S., Gross, R., Haas, A. H., Graf, J., Schwalbe, H., Mäntele, W., Simon, J., and Madej, G. (2005) Experimental support for the "E-pathway hypothesis" of coupled transmembrane e^- and H^+ transfer in dihemic quinol:fumarate reductase, *Proc. Natl. Acad. Sci. U.S.A.*, accepted for publication.
12. Haas, A. H., Sauer, U. S., Gross, R., Simon, J., Mäntele, W., and Lancaster, C. R. D. (2005) FTIR difference spectra of *Wolinella succinogenes* quinol:fumarate reductase support a key role of Glu C180 within the "E-pathway" hypothesis of coupled transmembrane electron and proton transfer, *Biochemistry 44*, 13949−13961.
13. Haas, A. H., and Lancaster, C. R. D. (2004) Calculated coupling of transmembrane electron and proton transfer in dihemic quinol: fumarate reductase, *Biophys. J. 87*, 4298−4315.
14. Behr, J., Hellwig, P., Mäntele, W., and Michel, H. (1998) Redox dependent changes at the heme propionates in cytochrome *c* oxidase from *Paracoccus denitrificans*: Direct evidence from FTIR difference spectroscopy in combination with heme propionate ^{13}C labeling, *Biochemistry 37*, 7400−7406.
15. Herzberg, G. (1962) *Molecular Spectra and Molecular Structure: II. Infrared and Raman Spectra of Polyatomic Molecules*, D. van Nostrand Company, Inc., Princeton, NJ.
16. Warren, M. J., and Scott, A. I. (1990) Tetrapyrrole assembly and modification into the ligands of biologically functional cofactors, *Trends Biochem. Sci. 15*, 486−491.

17. Kannangara, C. G., Gough, S. P., Bruyant, P., Hoober, J. K., Kahn, A., and von Wettstein, D. (1988) tRNA(Glu) as a cofactor in *δ*-aminolevulinate biosynthesis: Steps that regulate chlorophyll synthesis, *Trends Biochem. Sci. 13*, 139−143.
18. Baar, C., Eppinger, M., Raddatz, G., Simon, J., Lanz, C., Klimmek, O., Nandakumar, R., Gross, R., Rosinus, A., Keller, H., Jagtap, P., Linke, B., Meyer, F., Lederer, H., and Schuster, S. C. (2003) Complete genome sequence and analysis of *Wolinella succinogenes*, *Proc. Natl. Acad. Sci. U.S.A. 100*, 11690−11695.
19. Bronder, M., Mell, H., Stupperich, E., and Kröger, A. (1982) Biosynthetic Pathways of *Vibrio succinogenes* growing with fumarate as terminal electron acceptor and sole carbon source, *Arch. Microbiol. 131*, 216−223.
20. Lorenzen, J. P., Kröger, A., and Unden, G. (1993) Regulation of anaerobic respiratory pathways in *Wolinella succinogenes* by the presence of electron acceptors, *Arch. Microbiol. 159*, 477−483.
21. Sambrook, J., Fritsch, F. E., and Maniatis, T. (1989) *Molecular Cloning: A Laboratory Manual*, 2nd ed., Cold Spring Harbor Laboratory Press, Plainview, NY.
22. Simon, J., Gross, R., Ringel, M., Schmidt, E., and Kröger, A. (1998) Deletion and site-directed mutagenesis of the *Wolinella succinogenes* fumarate reductase operon, *Eur. J. Biochem. 251*, 418−426.
23. Lancaster, C. R. D. (2003) Crystallization of *Wolinella succinogenes* quinol:fumarate reductase, in *Membrane Protein Purification and Crystallization: A Practical Guide*, 2nd ed. (Hunte, C., Schägger, H., and von Jagow, G., Eds.) pp 219−228, Academic Press, San Diego, CA.
24. VanAken, T., Foxall-VanAken, S., Castleman, S., and Ferguson-Miller, S. (1986) Alkyl glycoside detergents: Synthesis and applications to the study of membrane proteins, *Methods Enzymol. 125*, 27−35.
25. Smith, P. K., Krohn, R. I., Hermanson, G. T., Mallia, A. K., Gartner, F. H., Provenzano, M. D., Fujimoto, E. K., Goeke, N. M., Olson, B. J., and Klenk, D. C. (1985) Measurement of protein using bicinchoninic acid, *Anal. Biochem. 150*, 76−85.
26. Kröger, A, and Innerhofer, A. (1976) The function of the *b* cytochromes in the electron transport from formate to fumarate of *Vibrio succinogenes*, *Eur. J. Biochem. 69*, 497−506.
27. Kröger, A., Winkler, E., Innerhofer, A., Hackenberg, H., and Schägger, H. (1979) The formate dehydrogenase involved in electron transport from formate to fumarate in *Vibrio succinogenes*, *Eur. J. Biochem. 94*, 465−475.
28. Kröger, A., Dorrer, E., and Winkler, E. (1980) The orientation of the substrate sites of formate dehydrogenase and fumarate reductase in the membrane of *Vibrio succinogenes*, *Biochim. Biophys. Acta 589*, 118−136.
29. Unden, G., Hackenberg, H., and Kröger, A. (1980) Isolation and functional aspects of the fumarate reductase involved in the phosphorylative electron transport of *Vibrio succinogenes*, *Biochim. Biophys. Acta 591*, 275−288.
30. Gast, P., Michalski, T. J., Hunt, J. E., and R., N. J. (1985) Determination of the amount and the type of quinones present in single crystals from reaction center protein from the photosynthetic bacterium *Rhodopseudomonas viridis*, *FEBS Lett. 179*, 325−328.
31. Unden, G. (1988) Differential roles for menaquinone and demethylmenaquinone in anaerobic electron transport of *E. coli* and their fnr-independent expression, *Arch. Microbiol. 150*, 499−503.
32. Lübben, M., and Morand, K. (1994) Novel prenylated hemes as cofactors of cytochrome oxidases. Archaea have modified hemes A and O, *J. Biol. Chem. 269*, 21473−21479.
33. Moss, D., Nabedryk, E., Breton, J., and Mäntele, W. (1990) Redox-linked conformational changes in proteins detected by a combination of infrared spectroscopy and protein electrochemistry. Evaluation of the technique with cytochrome *c*, *Eur. J. Biochem. 187*, 565−572.
34. Mäntele, W. (1996) Infrared and Fourier transform infrared spectroscopy, in *Biophysical Techniques in Photosynthesis* (Hoff, A. J., and Amesz, J., Eds.) pp 137−160, Kluwer, Dordrecht, The Netherlands.
35. Mäntele, W. (1993) Reaction-induced infrared difference spectroscopy for the study of protein function and reaction mechanisms, *Trends Biochem. Sci. 18*, 197−202.
36. Michal, G. (1999) Tetrapyrroles, in *Biochemical Pathways: An Atlas of Biochemistry and Molecular Biology* (Michal, G., Ed.) pp 68−74, John Wiley and Sons, Inc., New York.
37. Venyaminov, S. Y., and Kalnin, N. N. (1990) Quantitative IR spectrophotometry of peptide compounds in water (H_2O) solutions. I. Spectral parameters of amino acid residue absorption bands, *Biopolymers 30*, 1243−1257.
38. Li, X.-Y., Czernuszewicz, R. S., Kincaid, J. R., Su, Y. O., and Spiro, T. G. (1990) Consistent porphyrin force field. 1. Normal-mode analysis for nickel porphine and nickel tetraphenyiporphine from resonance Raman and infrared spectra and isotope shifts, *J. Phys. Chem. 94*, 31−47.
39. Berthomieu, C., Boussac, A., Mäntele, W., Breton, J., and Nabedryk, E. (1992) Molecular changes following oxidoreduction of cytochrome *b*559 characterized by Fourier transform infrared difference spectroscopy and electron paramagnetic resonance: Photooxidation in photosystem II and electrochemistry of isolated cytochrome *b*559 and iron protoporphyrin IX−bisimidazole model compounds, *Biochemistry 31*, 11460−11471.
40. Hellwig, P., Grzybek, S., Behr, J., Ludwig, B., Michel, H., and Mäntele, W. (1999) Electrochemical and ultraviolet/visible/infrared spectroscopic analysis of heme *a* and a_3 redox reactions in the cytochrome *c* oxidase from *Paracoccus denitrificans*: Separation of heme *a* and a_3 contributions and assignment of vibrational modes, *Biochemistry 38*, 1685−1694.
41. Schlereth, D. D., and Mäntele, W. (1992) Redox-induced conformational changes in myoglobin and hemoglobin: Electrochemistry and ultraviolet−visible and Fourier transform infrared difference spectroscopy at surface-modified gold electrodes in an ultra-thin-layer spectroelectrochemical cell, *Biochemistry 31*, 7494−7502.
42. Hellwig, P., Rost, B., Kaiser, U., Ostermeier, C., Michel, H., and Mäntele, W. (1996) Carboxyl group protonation upon reduction of the *Paracoccus denitrificans* cytochrome *c* oxidase: Direct evidence by FTIR spectroscopy, *FEBS Lett. 385*, 53−57.
43. Hellwig, P., Soulimane, T., Buse, G., and Mäntele, W. (1999) Electrochemical, FTIR, and UV/vis spectroscopic properties of the ba_3 oxidase from *Thermus thermophilus*, *Biochemistry 38*, 9648−9658.
44. Baymann, F., Robertson, D. E., Dutton, P. L., and Mäntele, W. (1999) Electrochemical and spectroscopic investigations of the cytochrome bc_1 complex from *Rhodobacter capsulatus*, *Biochemistry 38*, 13188−13199.
45. Breton, J., Bauscher, M., Berthomieu, C., Thibodeau, D. L., Andrianambinintsoa, S., Dejonghe, D., Mäntele, W., and Nabedryk, E. (1991) FTIR difference spectroscopy of menaquinone photoreduction in bacterial reaction centers, in *Spectroscopy of Biological Molecules* (Hester, R. E., and Girling, R. B., Eds.) pp 43−46, The Royal Society of Chemistry, Cambridge, U.K.
46. Breton, J., Burie, J.-R., Berthomieu, C., Thibodeau, D. L., Andrianambinintsoa, S., Dejonghe, D., Berger, G., and Nabedryk, E. (1992) Light-induced charge separation in photosynthetic bacterial reaction centers monitored by FTIR difference spectroscopy: The QA vibrations, in *The Photosynthetic Bacterial Reaction Center II* (Breton, J., and Verméglio, A., Eds.) pp 155−162, Plenum Press, New York.
47. Unden, G., Albracht, S. P. J., and Kröger, A. (1984) Redox potentials and kinetic properties of fumarate reductase complex from *Vibrio succinogenes*, *Biochim. Biophys. Acta 767*, 460−469.
48. Page, C. C., Moser, C. C., Chen, X., and Dutton, P. L. (1999) Natural engineering principles of electron tunnelling in biological oxidation−reduction, *Nature 402*, 47−52.

BI051034S